HHS Public Access

Author manuscript

Nat Immunol. Author manuscript; available in PMC 2020 February 05.

Published in final edited form as:

Nat Immunol. 2019 September ; 20(9): 1186–1195. doi:10.1038/s41590-019-0453-7.

Glycerol phosphate shuttle enzyme GPD2 regulates macrophage inflammatory responses

P. Kent Langston[1], **Aya Nambu**[1], **Jonathan Jung**[1,2], **Munehiko Shibata**[1], **H. Ibrahim Aksoylar**[1], **Jiahui Lei**[1], **Peining Xu**[3], **Mary T. Doan**[3], **Helen Jiang**[3], **Michael R. MacArthur**[1], **Xia Gao**[4], **Yong Kong**[5], **Edward T. Chouchani**[6], **Jason W. Locasale**[4], **Nathaniel W. Synder**[3], **Tiffany Horng**[1,7,*]

[1]Department of Genetics & Complex Diseases, Harvard T.H. Chan School of Public Health, Boston, Massachusetts

[2]School of Medicine,University of Glasgow, Glasgow, UK

[3]A.J. Drexel Autism Institute, Drexel University, Philadelphia, Pennsylvania

[4]Department of Pharmacology & Cancer Biology, Duke University School of Medicine, Durham, North Carolina

[5]Depart of Immunobiology, Yale University School of Medicine, New Haven, Connecticut

[6]Department of Cell Biology, Harvard Medical School, Boston, Massachusetts

[7]School of Life Sciences and Technology, ShanghaiTech University, Shanghai, China

Abstract

Macrophages are activated during microbial infection to coordinate inflammatory responses and host defense. Here we found that in macrophages activated by bacterial lipopolysaccharide (LPS), mitochondrial glycerol 3-phosphate dehydrogenase (GPD2) regulated glucose oxidation to drive inflammatory responses. GPD2, a component of the glycerol phosphate shuttle, boosted glucose oxidation to fuel the production of acetyl-coA, acetylation of histones and induction of genes encoding inflammatory mediators. While acute exposure to LPS drove macrophage activation, prolonged exposure to LPS triggered tolerance to LPS, in which macrophages induce immunosuppression to limit the detrimental effects of sustained inflammation. The shift in the inflammatory response was modulated by GPD2, which coordinated a shutdown of oxidative metabolism; this limited the availability of acetyl-coA for histone acetylation at genes encoding inflammatory mediators and thus contributed to the suppression of inflammatory responses. Therefore, GPD2 and the glycerol-phosphate shuttle integrate the extent of microbial stimulation

*Correspondence to: tsyhorng@shanghaitech.edu.cn.

Author Contributions

P.K.L. designed and performed experiments and analyzed data. J.J., A.N., M.S., H.I.A, and J.L. performed experiments and analyzed data. P.K.L. prepared figures, and P.K.L. and T.H. wrote the manuscript. T.H. supervised the project, including experimental design and data analysis. P.X., M.T.D., H.J., N.W.S., X.G., and J.W.L. performed metabolite profiling and provided related technical expertise. M.R.M. and Y.K. helped with data analysis. E.T.C. provided technical expertise.

Competing Interests

The authors declare no competing interests.

with glucose oxidation to balance the beneficial and detrimental effects of the inflammatory response.

Macrophages are key regulators of innate immunity and inflammation during microbial infection. Upon detection of the gram-negative bacterial component lipopolysaccharide (LPS), macrophages are activated (hereafter LPS activation) to coordinate the induction of innate and adaptive immune responses by producing chemoattractants and inflammatory cytokines. However, in response to overwhelming infection or protracted exposure to LPS, macrophages are initially activated but then shift to a tolerant state (hereafter LPS tolerance)[1, 2]. Tolerant macrophages mount a blunted response to further LPS challenge, and produce markedly lower amounts of inflammatory cytokines that contribute to the induction of whole-body immunosuppression. Such immunosuppression limits the detrimental effects of sustained inflammation, which otherwise damages multiple organ systems and leads to mortality[3]. Therefore, acute microbial infection elicits an inflammatory response that confers host defense, but persistent and overwhelming microbial infection triggers inflammation followed by a protracted period of tissue-protective immunosuppression[1, 2, 3].

Cellular metabolism is increasingly appreciated for its role in regulating macrophage activation and functions, as well as innate immunity and inflammation. Cellular metabolism interfaces with signal transduction and other regulatory processes, and genetic and pharmacological modulation of metabolism can influence macrophage activation and functions[4, 5]. In macrophages activated by IL-4, which orchestrate type 2 inflammatory responses like tissue repair and fibrosis, oxidative metabolism is increased to boost macrophage activation[4, 5, 6, 7, 8, 9]. For example, increased oxidative metabolism upregulates the production of citrate, a TCA cycle intermediate, which is used by ATP-citrate lyase (ACLY) to generate a nucleocytosolic pool of acetyl-CoA. Because acetyl-CoA is the metabolic substrate for histone acetylation, ACLY-dependent acetyl-CoA production links increased oxidative metabolism to enhanced expression of IL-4-inducible genes[6]. In contrast, a metabolic hallmark of LPS-stimulated macrophages is a robust shutdown of oxidative metabolism[4, 10, 11]. Such shutdown appears to be mediated by multiple mechanisms, including induction of iNOS and production of nitric oxide (NO), which modifies multiple complexes in the electron transport chain (ETC)[12, 13]; induction of IRG1 and its production of itaconate, a metabolite that inhibits complex II of the ETC[14]; and induction of reverse electron transport (RET), which counters oxidative phosphorylation[15]. In addition to respiratory shutdown, another metabolic hallmark of LPS-stimulated macrophages is the upregulation of aerobic glycolysis, the process by which glucose-derived pyruvate is shunted away from mitochondrial oxidative metabolism towards the production of lactate[4, 9, 10, 11, 16]. Therefore, despite reports of glucose oxidation in LPS-stimulated dendritic cells[13, 17], the paradigm is that LPS-stimulated macrophages divert glucose to aerobic glycolysis and shut down oxidative metabolism, but how such glucose utilization influences macrophage responses to LPS remains not well understood.

Here we show that during acute LPS exposure, macrophages upregulated glucose oxidation to support production of acetyl-CoA, thus increasing substrate availability for histone acetylation at the *Il6* and *Il1b* genes. However, there was a metabolic shift from increased to

decreased oxidative metabolism over the course of LPS exposure, and in tolerant macrophages, decreased oxidative metabolism limited the ability of glucose oxidation to support production of acetyl-CoA, thus contributing to the inability to induce *Il6* and *Il1b*. Such changes in glucose oxidation were regulated by GPD2, a rate-limiting enzyme in the glycerol phosphate shuttle (GPS). We propose that GPD2-mediated glucose oxidation has a unique role in integrating the duration and extent of microbial stimulation to the balance of inflammatory response induction and suppression.

Results

ACLY supports inflammatory gene induction during LPS activation

In IL-4-stimulated macrophages, increased oxidative metabolism bolsters macrophage activation in part by supporting the activity of ACLY, which produces a nucleocytosolic pool of acetyl-CoA that can be used for histone acetylation[6]. We investigated the role of ACLY in macrophages acutely exposed to LPS (0–3h of LPS stimulation, throughout the study), during the period of LPS activation. LPS stimulation of bone marrow-derived macrophages (BMDMs) for 0.5–2h increased the phosphorylation of S455 residue in ACLY (Fig. 1a), which is an activating phosphorylation[18], indicating that LPS signaling enhanced ACLY activation. Furthermore, treatment with the ACLY inhibitor SB-204990 attenuated LPS-inducible histone acetylation at *Il6* and *Il1b* gene promoters (Fig. 1b), as well as the LPS-inducible expression of *Il6* and *Il1b* mRNA, compared to no inhibitor (Fig. 1c). Two structurally distinct ACLY inhibitors, BMS-303141 and Medica16, similarly reduced LPS-induced histone acetylation and the expression of *Il6* and *Il1b* mRNA (Supplementary Fig. 1a,b), suggesting specificity in the effects of the ACLY inhibitors. Inhibition of p300 with the selective inhibitor C646 reduced LPS-inducible *Il6* and *Il1b* promoter histone acetylation and *Il6* and *Il1b* mRNA expression (Supplementary Fig. 1c,d), consistent with the idea that histone acetylation and histone acetyltransferases, including CBP/p300 in particular, support LPS-inducible gene expression[19, 20, 21, 22, 23]. These findings indicated that ACLY activity fueled histone acetylation and inflammatory gene induction in LPS-activated macrophages.

Glucose oxidation fuels inflammatory gene induction in LPS activation

Because ACLY-dependent production of acetyl-CoA depends on availability of the TCA cycle intermediate citrate and oxidative metabolism[24], that ACLY activity supported LPS-inducible inflammatory gene induction was in apparent conflict with the idea that LPS-stimulated macrophages shut down oxidative metabolism. Measurement of oxygen consumption indicated that a 1h LPS stimulation of BMDMs triggered a small, but significant and highly-reproducible increase in mitochondrial oxidative metabolism compared to no stimulation (Fig. 2a). Oxygen consumption began to decline after 2h, followed by a sustained decrease in oxygen consumption below that of unstimulated BMDMs between 4–24h (Supplementary Fig. 2a and data not shown), likely explaining previous conclusions that LPS-stimulated macrophages shut down oxidative metabolism. Because LPS stimulation enhances glucose utilization (Supplementary Fig. 2b and[4]), we tested if the increase in oxidative metabolism after 1h LPS stimulation could be fueled by glucose oxidation. Indeed, treatment with the glucose utilization inhibitor 2-deoxyglucose (2DG) abrogated such increase in oxidative metabolism, compared to no treatment (Fig. 2a).

To further test whether glucose oxidation supports acetyl-CoA production and inflammatory gene induction in LPS-activated BMDMs, we performed glucose isotope tracing using uniformly ^{13}C-labeled glucose. LPS stimulation for 1.5–3h enhanced the labeling of glucose-derived carbons into (m+2) citrate-isocitrate and (m+2) acetyl-CoA compared to no stimulation (Fig. 2b,c), indicating that glucose oxidation fueled acetyl-CoA production during LPS activation. Tracing glucose carbons all the way into histones indicated increased labeling of histones in LPS-stimulated BMDMs compared to no stimulation (Fig. 2d). 2DG treatment attenuated LPS-inducible histone acetylation at the promoters of *Il6* and *Il1b* (Fig. 2e) and expression of *Il6* and *Il1b* mRNA (Fig. 2f) compared to no 2DG treatment, indicating glucose metabolism supported histone acetylation. 2DG reduced the production of IL-6 in LPS-activated BMDMs (Fig. 2g), while production of mature IL-1β protein, which requires inflammasome activation in BMDMs[25], was not further examined. Incubation of BMDMs in glucose-free media also led to diminished induction of *Il6* and *Il1b* histone acetylation and mRNA expression (Supplementary Fig. 2c,d). These analyses suggested that availability of acetyl-CoA can be limiting for histone acetylation and inflammatory gene induction during LPS activation, and that LPS stimulation boosts glucose oxidation, leading to increased acetyl-CoA production, histone acetylation and inflammatory gene induction.

GPD2 regulates glucose utilization and oxidation in LPS activation

In the cytosolic phase of glucose oxidation, glucose-derived electrons are transferred to reduced nicotinamide adenine dinucleotide (NADH) at the step catalyzed by glyceraldehyde 3-phosphate dehydrogenase (GAPDH). The malate-aspartate shuttle (MAS) is thought to be ubiquitously deployed during glucose oxidation to transfer NADH to complex I of the ETC while regenerating cytosolic NAD^+ [24]. However, the ability of glucose carbons to label histones within 1.5h of labeling (Fig. 2d) relative to steady-state histone labeling in other contexts (~24h)[26, 27], suggested an alternative mechanism for rapidly mobilizing glucose oxidation in LPS-activated macrophages.

Applying global metabolomics to unstimulated and LPS-stimulated BMDMs, we identified the GPS, a glycolytic shunt that delivers glucose-derived electrons to the ETC, as a top metabolic pathway regulated during LPS activation (Fig. 3a). In the GPS, the NADH produced by GAPDH is used to reduce dihydroxyacetone phosphate (DHAP) to glycerol 3-phosphate (G3P); mitochondrial glycerol 3-phosphate dehydrogenase or GPD2 couples oxidation of G3P back to DHAP with reduction of its FAD cofactor to $FADH_2$, from which electrons flow downward through the ETC to drive mitochondrial respiration (Fig. 3b, Supplementary Fig. 3a and[24]). We found that LPS stimulation augmented GPD2 transcript and protein (Fig. 3c and Supplementary Fig. 3b). Furthermore, LPS stimulation of BMDMs increased the intrinsic activity of GPD2, compared to no stimulation, as assessed by seahorse extracellular flux analysis of G3P-driven oxygen consumption (Supplementary Fig. 3c).

Using Crispr-Cas9 genome editing, we generated *Gpd2*$^{-/-}$ mice, which were viable and fertile and appeared relatively normal (data not shown). *Gpd2*$^{-/-}$ BMDMs had normal expression of CD11b and F4/80 (Supplementary Fig. 3d), but lacked GPD2 protein and

activity as determined by immunoblotting (Fig. 3d) and seahorse extracellular flux analysis of G3P-driven oxygen consumption (Fig. 3e).

In glucose tracing experiments, 1.5–3h LPS stimulation of wild-type (*Gpd2*$^{+/+}$) BMDMs led to a marked increase in the abundance of total and (m+3) G3P (Fig. 3f), indicative of enhanced flux through the GPS, while in *Gpd2*$^{-/-}$ BMDMs, the abundance of total and (m +3) G3P was further increased (Fig. 3f), consistent with the accumulation of the GPD2 substrate in the absence of GPD2 activity. The 2DG-sensitive, LPS-inducible increase in oxidative metabolism apparent in wild-type BMDMs (Fig. 2a and Fig. 3g) was diminished in *Gpd2*$^{-/-}$ BMDMs (Fig. 3g), indicating a role for GPD2 in mediating glucose oxidation in LPS-activated macrophages. Importantly, the ability of LPS to augment glucose uptake was impaired in *Gpd2*$^{-/-}$ BMDMs compared to wild-type BMDMs (Fig. 3h), indicating that GPS activity is rate-limiting for glucose utilization in LPS-activated macrophages. Compared to wild-type BMDMs, *Gpd2*$^{-/-}$ BMDMs had less LPS-inducible glucose labeling into many glycolytic and TCA intermediates (Supplementary Fig. 4) and aerobic glycolysis (Fig. 3i), in line with reduced LPS-inducible glucose utilization and oxidation. These observations indicated that the GPS was a critical regulator of glucose utilization and oxidation in LPS-activated macrophages.

Impaired inflammatory gene induction in LPS-activated *Gpd2*$^{-/-}$ BMDMs

We next investigated how reduced glucose utilization and oxidation in *Gpd2*$^{-/-}$ BMDMs affected LPS activation. LPS-inducible labeling of glucose carbons into citrate and acetyl-CoA was reduced in *Gpd2*$^{-/-}$ BMDMs compared to wild-type BMDMs (Fig. 4a,b). LPS-inducible histone acetylation at the *Il6* and *Il1b* promoters was also attenuated in *Gpd2*$^{-/-}$ BMDMs (Fig. 4c), leading to diminished *Il6* and *Il1b* mRNA expression (Fig. 4d) and IL-6 production (Fig. 4e), compared to wild-type BMDMs. Together these findings indicated that in LPS-activated macrophages, GPS activity boosted glucose oxidation, leading to enhanced carbon substrate availability for histone acetylation and increased inflammatory gene induction (Supplementary Fig. 5a).

Glucose use suppresses inflammatory gene induction in LPS tolerance

During the course of LPS exposure, there is a transition from LPS activation to tolerance[1, 2]. Acute LPS stimulation (0–3h) of BMDMs led to induction of *Il6* and *Il1b* mRNA during the period of LPS activation, while prolonged LPS stimulation (12–24h) led to an inability to induce *Il6* and *Il1b* mRNA after a second LPS challenge during the period of LPS tolerance (Supplementary Fig. 6a,b and[1, 2]). Our data indicated that such shift from inflammatory response induction to suppression was accompanied by a shift from increased to decreased oxidative metabolism (Supplementary Fig. 2a). Because increased oxidative metabolism supports inflammatory gene induction during LPS activation, we tested whether the decrease in oxidative metabolism in LPS-tolerant BMDMs limited the availability of acetyl-CoA for histone acetylation and contributed to suppression of inflammatory gene induction. In contrast to naïve BMDMs, in which a 3h LPS stimulation induced glucose conversion into citrate and acetyl-CoA, LPS did not drive glucose conversion into citrate and acetyl-CoA in BMDMs tolerized by 24h LPS stimulation (Fig. 5a,b), suggesting reduced LPS-induced glucose oxidation and acetyl-CoA production in tolerant macrophages.

Serendipitously, we found that treating BMDMs with 2DG during a 12h LPS tolerance induction led to a rescue of oxygen consumption compared to no 2DG treatment (Fig. 5c). 2DG treatment during a 24h LPS tolerance induction was also associated with recovery of *Il6* and *Il1b* promoter histone acetylation, *Il6* and *Il1b* mRNA expression and IL-6 production compared to no 2DG treatment (Fig. 5d,e,f). These findings indicated that glucose utilization was necessary for optimal inhibition of oxidative metabolism and suppression of inflammatory gene induction during LPS tolerance. We next investigated the effects of 2DG treatment on LPS signaling. NF-kB and IRF3, which are the master regulators of the LPS-inducible transcriptional response, were robustly activated by LPS in unstimulated BMDMs, but poorly activated in BMDMs tolerized by 24h LPS stimulation, as indicated by degradation and resynthesis of IκBα and activating phosphorylation of IRF3, respectively (Fig. 5g,h). 2DG treatment during such LPS tolerance induction had marginal effects on activation of NF-kB and IRF3 (Fig. 5g,h), compared to no 2DG treatment, indicating that the effect of 2DG in recovering *Il6* and *Il1b* mRNA might not be due to a general perturbation of LPS signaling. Together these findings indicated that during prolonged LPS exposure, glucose utilization was necessary for optimal shutdown of oxidative metabolism and suppression of histone acetylation and inflammatory gene induction.

Rescued inflammatory gene induction in tolerant *Gpd2*$^{-/-}$ BMDMs

Next we tested the role of GPD2-GPS activity in the induction of LPS tolerance. In *Gpd2*$^{-/-}$ BMDMs tolerized by 24h LPS stimulation, tolerance-associated inhibition of oxygen consumption was attenuated compared to wild-type counterparts (Fig. 6a), indicating that GPD2 was necessary for optimal oxidative metabolism shutdown. Likewise, tolerance-associated suppression of H4Ac and H3K27Ac at the *Il6* and *Il1b* promoters (Fig. 6b), *Il6* and *Il1b* mRNA expression (Fig. 6c) and IL-6 production (Fig. 6d) was attenuated in *Gpd2*$^{-/-}$ BMDMs compared to wild-type counterparts, indicating that GPD2 activity was needed for optimal suppression of inflammatory responses. That GPD2 deficiency increased both oxidative metabolism and inflammatory gene expression also linked shutdown of oxidative metabolism to inflammatory gene suppression during tolerance.

Recapitulating our findings in *Gpd2*$^{-/-}$ BMDMs, treatment with the GPD2 inhibitor iGP-1 attenuated the ability of acute LPS stimulation (0–3h) to induce oxidative metabolism, *Il6* and *Il1b* promoter histone acetylation and *Il6* and *Il1b* mRNA expression during LPS activation (Supplementary Fig. 7a–c), but rescued the tolerance-associated shutdown of oxidative metabolism and suppression of *Il6* and *Il1b* promoter histone acetylation and *Il6* and *Il1b* mRNA expression triggered by prolonged LPS stimulation (12–24h) (Supplementary Fig. 7d–f), compared to no inhibitor treatment. Of note, LPS-inducible degradation and resynthesis of IκBα and activating phosphorylation of IRF3 in naïve or tolerant *Gpd2*$^{-/-}$ BMDMs was similar to that of wild-type counterparts (Fig. 6e,f). Therefore, GPD2 did not exert broad effects on LPS signaling to influence histone acetylation and inflammatory gene induction during LPS stimulation.

GPD2 regulates RET in tolerant macrophages

We next investigated the mechanisms by which GPD2-GPS activity mediated shutdown of oxidative metabolism during LPS tolerance. Multiple factors are thought to modulate such shutdown, including induction of iNOS, IRG1 and RET[12, 13, 14, 15], as well as repression of the TCA cycle enzyme IDH1, which allows carbon flux to be shunted from the TCA cycle towards itaconate production. Over a time course of LPS stimulation, wild-type and *Gpd2*$^{-/-}$ BMDMs had similar expression of *Nos2*, *Irg1* and *Idh1* mRNA (Supplementary Fig. 8a) and levels of itaconate (Supplementary Fig. 8b).

We next investigated a potential role for GPD2-mediated glucose oxidation in regulating RET during LPS tolerance. In contrast to forward electron transport (FET), which is the normal operation of the ETC, RET is a consequence of overwhelming electron influx into the ETC, which leads to the saturation of electron transport capacity and creates thermodynamic conditions that allow electron flow in reverse[28]. Therefore, we tested whether sustained GPS activity during prolonged LPS exposure could overwhelm forward electron transport capacity leading to RET, which reduced TCA cycling to limit acetyl-CoA production and contribute to inflammatory gene suppression (Supplementary Fig. 8c). In contrast to FET, in which treatment with the complex I inhibitor rotenone enhances superoxide production, RET-associated reverse electron flow at complex I leads to increased production of superoxide that is sensitive to rotenone[29, 30]. While rotenone treatment increased the levels of superoxide in wild-type unstimulated BMDMs, it decreased the levels of superoxide in wild-type BMDMs tolerized by 12h LPS stimulation (Fig. 7a,b), indicating RET was induced after prolonged LPS exposure. The ability of rotenone to reduce superoxide was diminished in *Gpd2*$^{-/-}$ tolerant BMDMs compared wild-type counterparts (Fig. 7a,b), indicating that GPD2 contributed to tolerance-associated RET. Similarly, rotenone stimulated superoxide levels in 2DG-treated tolerant BMDMs compared to no 2DG treatment (Fig. 7a,b), indicating complete prevention of tolerance-associated RET.

Compared to robust NADH oxidation to NAD^+ at complex I during FET, complex I-associated NADH oxidation is attenuated during RET[28] (Supplementary Fig. 8c). Using an assay that detects NAD(P)H autofluorescence in real-time, and in which rotenone acutely blocks complex I activity to reveal NADH oxidation at complex I[31], we found that rotenone robustly enhanced NADH in wild-type unstimulated BMDMs, indicative of robust FET, and modestly enhanced NADH in wild-type BMDMs tolerized by 12h LPS stimulation (Fig. 7c,d), indicative of reduced FET and/or increased RET, because the net NADH amount is determined by the relative magnitudes of FET and RET. However, rotenone did not differentially modulate NADH levels between unstimulated and tolerant *Gpd2*$^{-/-}$ BMDMs or between 2DG-treated and untreated wild-type tolerant BMDMs (Fig. 7c,d), indicating that GPD2 deficiency or 2DG treatment mitigated the reduction of FET and/or the induction of RET during tolerance. These results indicated that sustained GPD2 activity during prolonged LPS exposure overwhelmed the ETC to trigger RET and perturb NADH oxidation, and suggested how GPD2 deficiency could lead to a recovery of oxidative metabolism, acetyl-CoA production, histone acetylation and inflammatory gene induction in tolerant macrophages. Therefore, GPS activity supports inflammatory response induction during acute LPS exposure and inflammatory response suppression during prolonged LPS

exposure, acting as a rheostat to link the duration of LPS exposure to the balance of inflammatory response induction and suppression (Supplementary Fig. 5b).

GPD2 activity suppresses inflammatory responses during septic shock

To ask whether GPD2 regulated inflammatory responses *in vivo* we used a model of *in vivo* LPS tolerance, in which a sub-lethal dose of LPS protects against septic shock triggered by a subsequent, lethal dose of LPS. In contrast to counterparts that did not receive the sub-lethal LPS pre-treatment, wild-type mice receiving the pre-treatment markedly suppressed circulating amounts of IL-6, as detected 6h after lethal LPS challenge (Fig. 8a). Compared to wild-type counterparts, *Gpd2*$^{-/-}$ mice receiving the pretreatment had increased circulating amounts of IL-6, indicating attenuated suppression of inflammatory responses (Fig. 8a). Furthermore, the drop in body temperature induced 6h after lethal LPS challenge was exaggerated in *Gpd2*$^{-/-}$ mice compared to wild-type mice (Fig. 8b), indicating an augmented response to lethal LPS challenge. Finally, wild-type mice that received a sublethal LPS pretreatment survived the subsequent lethal LPS challenge, while *Gpd2*$^{-/-}$ mice succumbed (Fig. 8c), suggesting a profound defect in LPS tolerance and immunosuppression in the absence of GPD2. Collectively the data indicates that GPD2 suppressed inflammatory responses to protect against a drop in body temperature and mortality during septic shock.

Discussion

In this study we make several findings regarding the role of glucose utilization in controlling the fate of macrophages exposed to LPS. We showed that oxidative metabolism was increased in LPS-activated BMDMs, fueling the production of acetyl-CoA to provide carbon substrate for histone acetylation at the *Il6* and *Il1b* promoters. Our findings defined a new role for glucose utilization in LPS-stimulated macrophages—namely glucose oxidation—as well as an underpinning basis by which such glucose utilization drove LPS activation. We also showed that the acetyl-CoA-producing enzyme ACLY was a key regulator of this process that supported histone acetylation and inflammatory gene induction during LPS activation.

We identified GPD2 and the GPS as key regulators of glucose oxidation in LPS-stimulated macrophages. Like the MAS, the GPS regenerates cytosolic NAD^+ to maintain redox balance during glucose oxidation, but unlike the MAS, GPS activity is restricted to a limited number of tissues, because GPD2 is expressed in a tissue-specific manner[32, 33]. The role of GPD2 in macrophages is unknown, except that its biochemical activity is increased after microbial infection[34]. Here we showed that LPS stimulation increased flux through the GPS by augmenting glucose utilization (which stimulates substrate delivery to the GPS), GPD2 expression and the intrinsic activity of GPD2. Such increase of GPS flux is noteworthy given that macrophages can deploy the malate-aspartate shuttle to maintain glucose oxidation[35], and suggests a non-redundant role for the GPS in regulating macrophage responses to LPS (see below).

Although shutdown of oxidative metabolism is a metabolic hallmark of LPS-stimulated macrophages, its role in modulating macrophage responses to LPS had been unclear[4, 10, 36].

Here we showed that such shutdown occurred at 12–24h after LPS stimulation, after the initial increase in oxidative metabolism, and contributed to reduced acetyl-CoA production, histone acetylation and inflammatory gene induction in tolerant macrophages. We propose that shutdown of oxidative metabolism is central to metabolic reprogramming during LPS tolerance, while induction of aerobic glycolysis is presumably a compensatory mechanism to support cellular bioenergetics (i.e., ATP production) in the face of oxidative metabolism shutdown.

We found that GPD2 and the GPS were important regulators of tolerance-associated shutdown of oxidative metabolism. Inhibiting glucose utilization or GPD2 deficiency was sufficient for partial restoration of oxidative metabolism, leading to a partial recovery of histone acetylation and inflammatory gene induction in tolerant macrophages, as well as increased IL-6 production and mortality during septic shock. We propose a model in which GPS activity influences oxidative metabolism to modulate a shift from inflammatory response induction to suppression. During acute LPS exposure, GPS activity drives FET and acetyl-CoA production to enhance histone acetylation and inflammatory gene induction, but during prolonged LPS exposure, sustained GPS activity eventually saturates electron transport capacity to trigger RET and limit acetyl-CoA production for histone acetylation and inflammatory gene induction. Therefore, GPS activity triggered RET as a consequence of its initial boost of FET, allowing the GPS to integrate the duration of LPS exposure with the activity of the ETC. In this manner, GPS activity supported inflammatory responses after acute microbial exposure, but contributed to inflammatory response suppression after prolonged microbial exposure. Inflammation confers host defense at the expense of tissue damage and must be carefully regulated to balance its beneficial and detrimental effects, and GPS activity, by integrating the extent of microbial exposure to inflammatory response induction versus suppression, may provide one such balancing mechanism.

Our detailed metabolic analyses implicated histone acetylation at inflammatory genes as a key target by which GPD2 regulates inflammatory gene expression. In contrast, we found no broad effects of GPD2 deficiency on LPS-inducible NF-kB and IRF3 activation, or LPS-inducible gene expression as assessed by RNA-seq (data not shown). However, we do not exclude the possibility that GPD2 activity impinges on specific aspects of LPS signaling to contribute to its regulation of inflammatory gene expression. For example, GPD2-mediated glucose oxidation could influence the expression of specific signaling proteins, via effects on promoter histone acetylation and protein acetylation, an effect non-exclusive with its modulation of histone acetylation at inflammatory genes. Additionally, how GPD2-mediated glucose oxidation and acetyl-CoA production can modulate histone acetylation and the expression of a subset of LPS-inducible genes remains unclear. One possibility is that ACLY is recruited to chromatin, producing a local pool of acetyl-CoA that regulates histone acetylation in a gene-specific manner. Precedence for such gene-specific association and regulation has been established by the metabolic machinery that produces S-adenosylmethionine, the substrate for histone and DNA methylation[37].

Our findings indicate that increased oxidative metabolism is a common feature of LPS- and IL-4-activated macrophages, and that one consequence of this process is enhanced provision of acetyl-CoA, which is otherwise limiting for histone acetylation and inducible gene

expression. Therefore, polarizing signals like LPS and IL-4 mobilize oxidative metabolism to drive optimal gene induction and macrophage activation. In the case of LPS-stimulated macrophages, this process is further exploited to eventually influence oxidative metabolism shutdown and inflammatory gene suppression. In this regard, our conclusions appear in conflict with those of a recent study showing that RET-associated ROS production drives *Il1b* induction[16]. However, that study did not perform a kinetic analysis of LPS stimulation, while in our study, we examined glucose oxidation, oxidative metabolism, FET/RET and inflammatory gene induction or suppression over a time course, allowing us to address how dynamic changes to oxidative metabolism and FET/RET could affect the dynamic changes to inflammatory gene induction or suppression that occur over the course of LPS exposure.

In conclusion, we propose that GPD2-GPS-mediated glucose oxidation has a unique, non-redundant role in optimal control of inflammatory gene induction and suppression. Compared with the MAS, GPS activity may allow for rapid and robust glucose oxidation that drives ETC flux and inflammatory gene expression during LPS activation, but in the event of sustained LPS exposure, contributes to RET induction. Therefore, deployment of the GPS in the high metabolic state of LPS-stimulated macrophages enables GPD2 activity to act as a rheostat that couples duration of LPS exposure to ETC directionality to enable appropriate modulation of inflammatory response induction and suppression.

Methods

BMDM culture.

BMDMs from male and female mice were differentiated and cultured as described previously[38]. For LPS activation (0–3h post-LPS), BMDMs were stimulated with 100 ng/mL LPS (LPS Ultra-Pure, Sigma-Aldrich). All of the metabolic parameters associated with LPS activation, including glucose uptake and oxidation, glucose tracing into TCA intermediates and acetyl-CoA, ACLY phosphorylation, glucose labeling into histones, and promoter histone acetylation, were assessed at early time points after LPS stimulation (0–3 h), while the downstream consequences of such metabolic events, i.e., inflammatory gene induction and cytokine production, were assessed at 3 h after LPS stimulation. For LPS tolerance (12–28h post-LPS), BMDMs were challenged with 100 ng/mL LPS for 24h to induce tolerance (T), washed, and then rechallenged with 10 ng/mL LPS (T+LPS) for the desired amount of time. In such experiments, unstimulated (naïve) BMDMs were incubated in media for 24h (U), washed, and challenged with 10 ng/mL LPS (U+LPS) to provide responsive-cell controls. Pharmacological inhibition of ACLY (ACLYi, 80–160 μM; SB-204990, Tocris, United Kingdom), glucose utilization (2DG, 5–10 mM; 2-deoxy-glucose, Sigma-Aldrich), and GPD2 (GPD2i, 300 μM; iGP-1, Calbiochem) was achieved by pretreating BMDMs with for 1h prior to LPS activation. For rescue of tolerance, BMDMs were pretreated for 1h prior to activation, but drugs were not added back after wash before restimulation. Additional drugs include the ACLY inhibitors BMS-303141 and Medica16 and the p300 inhibitor C646.

Seahorse assays.

Basal and LPS-induced changes in oxygen consumption (OCR) and extracellular acidification (ECAR) rates were measured with a Seahorse XF96 Extracellular Flux Analyzer (Agilent). For experiments in intact cells, assays were performed in Seahorse XF Assay Medium supplemented with glucose (11 mM) and adjusted to pH 7.4 with NaOH. Mix-wait-measure durations were set to 3, 2, and 3 minutes, respectively. For the MitoStress Test, oligomycin, FCCP, and rotenone/antimycin A were sequentially injected to achieve final concentrations of 1, 1.5, and 2 μM. Glycolysis Tests were performed in unsupplemented XF Assay Medium, and glucose, oligomycin, and 2DG were sequentially injected to achieve final concentrations of 11 mM, 1 μM, and 500 mM, respectively. Non-mitochondrial OCR was subtracted from the mean pre-oligomycin OCR and the mean post-FCCP OCR to calculate Basal and Maximal mitochondrial OCR, respectively. For experiments in permeabilized cells[39], assays were performed in mannose sucrose buffer supplemented with 0.1% BSA and adjusted to pH 7.2 with KOH (MAS-BSA Buffer). Cells were permeabilized by injection of perfringolysin O (PMP reagent, Agilent) in the XF96 Analyzer, and specific mitochondrial enzyme activities were determined by measuring State 3 respiration in the presence of substrate/inhibitors/ADP, followed by sequential injection of oligomycin and antimycin A. GPD2 activity was measured as the change in OCR induced by injection of 10 mM *sn*-glycerol 3-phosphate (G3P, Sigma-Aldrich), 1 mM ADP, and 2 μM Rotenone. After each experiment, OCR and ECAR values from six or eight replicate wells were normalized to DNA content in each well by Hoechst 33342 staining (Life Technologies, Carlsbad, CA).

Steady-state metabolomics and relative metabolic flux.

For steady-state analysis of metabolic networks, BMDMs were stimulated for the desired period of time and then lysed and polar metabolites extracted using 80:20 methanol:water (HPLC-grade, Sigma-Aldrich). Extracts were dried under nitrogen gas followed by LC-MS (Beth Israel Deaconess Medical Center Mass Spectrometry Facility) to monitor targeted metabolites from a library of 300 species, including those involved in glycolysis, the glycerol 3-phosphate shuttle, and the TCA cycle. MS peak areas were normalized to median and sample protein concentrations, and LPS-induced fold-change data was run through the Metaboanalyst 2.0 web-based pipeline to visualize metabolic pathway enrichment. For relative metabolic flux analysis, unstimulated and LPS-stimulated BMDMs were washed with glucose-free medium and then labeled with 2 g/L $^{13}C_6$-gluose (Cambridge Isotope Laboratories) in complete medium (10% dialyzed FBS) for 30 min. Metabolites were extracted, dried, and run as in[40]. Normalized peak data was analyzed for percent labeling of glucose into each possible isotopologue of species in glycolysis, the glycerol 3-phosphate shuttle, and the TCA cycle. Steady-state and metabolic flux analyses were performed on triplicate or quadruplicate cell cultures. Precise *n* for each metabolite is indicated in figure legends.

Acyl-CoA mass spectrometry.

Unstimulated and LPS-stimulated quadruplicate cultures of BMDMs were washed with glucose-free medium and then labeled with 2 g/L $^{13}C_6$-gluose (Cambridge Isotope

Laboratories) in complete medium (10% dialyzed FBS) for 30 min. Cells were then lysed in 800 μL ice-cold 10% trichloroacetic acid and extracted as previously described[41]. Analysis by LC-high resolution MS was conducted on an Ultimate 3000 UHPLC coupled to a Q Extractive Plus operating in the positive ion mode as previously described[42]. Isotopologue analysis was conducted using FluxFix[43].

Glucose tracing into histones.

Glucose tracing into histones was done following an established protocol[26]. In the last 1.5h of stimulation, BMDMs were labeled with $^{14}C_6$-glucose followed by acid extraction of acetylated histones. Radiolabel incorporation was assessed in technical duplicates by scintillation counting and normalized to total protein concentration.

Glucose uptake.

Basal and LPS-inducible glucose uptake in BMDMs was measured using ^{3}H-deoxy-D-glucose (2-^{3}H[G]) (PerkinElmer) in KRBH buffer. Counts per minute (cpm) were measured in triplicate cell cultures and then normalized to protein concentration in each sample.

NADH analysis.

For NADH autofluorescence, BMDMs were excited at 340/26 nm on a Nikon Eclipse Ti-S microscope. The emitted signal was collected using a 460/80 nm bandpass filter. Autofluorescence was analyzed for at least 100 cells per condition, per timpepoint using Fiji image processing software. Duplicate cell cultures were analyzed for each condition tested.

Chromatin immunoprecipitation.

Acetylation at inflammatory gene promoters was measured by chromatin immunoprecipitation (ChIP) assay. Promoters are defined as the region between −500 bp and the transcription start site. Antibodies used were as follows: acetylated H3 (Millipore 06–599), acetylated H3K27 (Abcam ab4729), acetylated H4 (Millipore 06–866), and IgG (Santa Cruz, Dallas, TX, SC-2027). Fold enrichment was calculated as ChIP signals normalized to input. Technical triplicates were analyzed for each condition tested.

Gene expression.

RNA was isolated from BMDMs using RNA-Bee (Tel-Test) according to the manufacturer's protocol. cDNA synthesis was performed using a High Capacity cDNA Reverse Transcription Kit (Applied Biosystems). qPCRs were run on a Bio-Rad C1000 Thermalcycler, and expression of target genes was calculated by the Δ/Δ CT method using CFX Manger Software (Bio-Rad). Relative expression values for target genes were calculated by normalization to expression of hypoxanthine phosphoribosyltransferase (HPRT). Duplicate cell cultures were analyzed for each condition tested.

Generation of *Gpd2*$^{-/-}$ mice.

Gpd2$^{-/-}$ mice were generated on the C57BL/6J background using a gRNA targeting exon 6 of *mGPD2* (oligo 1: CACCGCGTACCGTCATAGTAGACAA, oligo 2: CGCATGGCAGTATCATCTGTTCAAA). gRNA and Cas9 RNA were injected into eggs

followed by implantation into recipient female mice at the BWH Transgenic Core. Mice were backcrossed two times to C57BL/6 mice. BMDMs from two independently generated lines were used with similar results.

Mice.

Wild-type C57BL/6J mice (The Jackson Laboratory) and whole-body *Gpd2*−/− mice were maintained under specific pathogen-free conditions at the Harvard T.H. Chan School of Public Health in accordance with Institutional Animal Care and Use Committee (IACUC) guidelines. Male and female mice were used for *in vivo* LPS tolerance experiments and as a source of bone marrow for BMDM culture between 6 and 12 weeks of age. All protocols were approved by the IACUC of Harvard Medical School. In the in vivo LPS tolerance experiments, wild-type and $Gpd2^{-/-}$ mice were injected with vehicle (saline) or 3 mg/kg LPS via intraperitoneal injection (IP) followed by 30 mg/kg LPS IP 24h later. Serum IL-6 and internal body temperature (TH-5 Thermalert Clinical Monitoring Thermometer, Physitemp) were measured for 6 h after lethal LPS challenge. Survival of wild-type and $Gpd2^{-/-}$ mice that received both challenges was recorded as an indication of differential endotoxin tolerance *in vivo*.

Immunoblot and enzyme-linked immunosorbent assays.

For immunoblotting, BMDMs were lysed in 1% NP-40 buffer or RIPA buffer, and protein concentration was determined using the Bradford method or micro BCA assay (Pierce). Primary antibodies used were anti-phospho-ACLY(S455) and anti-ACLY (1:1000, Cell Signaling), anti-GPD2 (1:800, ProteinTech), anti-IκB (1:1000, Santa Cruz), anti-phospho-IRF3 (1:1000, Cell Signaling), and anti-α-tubulin (1:5000, Sigma-Aldrich). For ELISA, cell culture supernatants and mouse whole blood were spun down (5 min at 400 *g* and 20 min at 13,000 *g*, respectively), diluted appropriately in 5% BSA, and assayed for IL-6 using BioLegend Standard ELISA kits according to the manufacturer's protocols. For in vitro LPS tolerance experiments, cell culture supernatants in the T and T+L conditions were collected after LPS washout and rest or restimulation for 4h (refer to Fig 5a; time of collection indicated by "Assay"), allowing for measurement of IL-6 produced during tolerance rather than activation. Supernatants were analyzed from duplicate or quadruplicate cell cultures, indicated by *n* in figure legends. Full scans of western blots can be found in Supplementary Fig. S9–11.

Flow cytometry.

Efficiency of macrophage differentiation from bone-marrow-derived progenitors was determined by staining D7 BMDMs with anti-F4/80 (BM8) and anti-CD11b (M1/70) antibodies (BD Bioscience) for 30 min at 4°C in FACS buffer (2% FCS), followed by washes and fixation in 2% ultrapure paraformaldehyde. Mitochondrial superoxide was measured by MitoSox (Life Technologies) staining according to the manufacturer's protocol. Briefly, BMDMs were left unstimulated or stimulated with LPS for the indicated times and then labeled with 2.5 μM MitoSox Red in the final 15 minutes of treatment, followed by washout and no fixation. Mean fluorescence intensity of MitoSox in the PE channel was measured to determine levels of mitochondrial superoxide at the time of labeling. Duplicate cell culture samples were run for each condition in every experiment. All

samples were acquired on a BD FACS Fortessa flow cytometer, and FlowJo software (v10.4) was used to analyze data.

Statistical analysis.

Data are shown as mean or mean +/− s.e.m. or s.d., as indicated in figure legends. Statistical significance was determined by a two-tailed Student's *t*-test, 2way ANOVA with Sidak's multiple comparisons test, or Mantel-Cox test using Prism software (GraphPad), as indicated in figure legends. All statistical tests were performed using GraphPad Prism, except for pathway enrichment analysis of steady-state metabolite profiling, for which Metaboanalyst was used to generate statistics. *, **, ***, and **** in figures denote p value ≤0.05, 0.01, 0.001, and 0.0001, respectively.

Reporting Summary.

Further information on research design is available in the Nature Research Reporting Summary linked to this article.

Data Availability

The data that supports the findings of this study are available from the corresponding author upon request.

Supplementary Material

Refer to Web version on PubMed Central for supplementary material.

Acknowledgements

J.J. was supported by the British Society for Immunology and T.H. by NIH grant R01AI102964. N.W.S. was supported by NIH R03 HD092630, X.G. by the Canadian Institutes of Health Research (CIHR) reference number 146818, and E.T.C. by the Claudia Adams Barr Program. We thank J.F. Mohan for helpful suggestions for Crispr-Cas9 genome editing, L.B. Sullivan for technical advice on the GPD2 Seahorse assay, R.L.S. Goncalves for technical advice on the NAD(P)H autofluorescence assay, and H. Affronti and K.E. Wellen for sharing reagents.

References

1. Foster SL & Medzhitov R Gene-specific control of the TLR-induced inflammatory response. Clin Immunol 130, 7–15 (2009). [PubMed: 18964303]
2. Seeley JJ & Ghosh S Molecular mechanisms of innate memory and tolerance to LPS. J Leukoc Biol 101, 107–119 (2017). [PubMed: 27780875]
3. Hotchkiss RS, Monneret G & Payen D Sepsis-induced immunosuppression: from cellular dysfunctions to immunotherapy. Nat Rev Immunol 13, 862–874 (2013). [PubMed: 24232462]
4. O'Neill LA & Pearce EJ Immunometabolism governs dendritic cell and macrophage function. J Exp Med 213, 15–23 (2016). [PubMed: 26694970]
5. Jung J, Zeng H & Horng T Metabolism as a guiding force for immunity. Nat Cell Biol 21, 85–93 (2019). [PubMed: 30602764]
6. Covarrubias AJ et al. Akt-mTORC1 signaling regulates Acly to integrate metabolic input to control of macrophage activation. Elife 5 (2016).
7. Liu PS et al. α-ketoglutarate orchestrates macrophage activation through metabolic and epigenetic reprogramming. Nat Immunol 18, 985–994 (2017). [PubMed: 28714978]
8. Vats D et al. Oxidative metabolism and PGC-1beta attenuate macrophage-mediated inflammation. Cell Metab 4, 13–24 (2006). [PubMed: 16814729]

9. Lacy-Hulbert A & Moore KJ Designer macrophages: oxidative metabolism fuels inflammation repair. Cell Metab 4, 7–8 (2006). [PubMed: 16814727]
10. Langston PK, Shibata M & Horng T Metabolism Supports Macrophage Activation. Front Immunol 8, 61 (2017). [PubMed: 28197151]
11. Hard GC Some biochemical aspects of the immune macrophage. Br J Exp Pathol 51, 97–105 (1970). [PubMed: 5434449]
12. Drapier JC & Hibbs JB Differentiation of murine macrophages to express nonspecific cytotoxicity for tumor cells results in L-arginine-dependent inhibition of mitochondrial iron-sulfur enzymes in the macrophage effector cells. J Immunol 140, 2829–2838 (1988). [PubMed: 2451695]
13. Everts B et al. Commitment to glycolysis sustains survival of NO-producing inflammatory dendritic cells. Blood 120, 1422–1431 (2012). [PubMed: 22786879]
14. Lampropoulou V et al. Itaconate Links Inhibition of Succinate Dehydrogenase with Macrophage Metabolic Remodeling and Regulation of Inflammation. Cell Metab 24, 158–166 (2016). [PubMed: 27374498]
15. Mills EL et al. Succinate Dehydrogenase Supports Metabolic Repurposing of Mitochondria to Drive Inflammatory Macrophages. Cell 167, 457–470.e413 (2016). [PubMed: 27667687]
16. Cheng SC et al. Broad defects in the energy metabolism of leukocytes underlie immunoparalysis in sepsis. Nat Immunol 17, 406–413 (2016). [PubMed: 26950237]
17. Everts B et al. TLR-driven early glycolytic reprogramming via the kinases TBK1-IKKε supports the anabolic demands of dendritic cell activation. Nat Immunol 15, 323–332 (2014). [PubMed: 24562310]
18. Berwick DC, Hers I, Heesom KJ, Moule SK & Tavare JM The identification of ATP-citrate lyase as a protein kinase B (Akt) substrate in primary adipocytes. J Biol Chem 277, 33895–33900 (2002). [PubMed: 12107176]
19. Sacta MA et al. Gene-specific mechanisms direct glucocorticoid-receptor-driven repression of inflammatory response genes in macrophages. Elife 7 (2018).
20. Hargreaves DC, Horng T & Medzhitov R Control of inducible gene expression by signal-dependent transcriptional elongation. Cell 138, 129–145 (2009). [PubMed: 19596240]
21. Smale ST & Natoli G Transcriptional control of inflammatory responses. Cold Spring Harb Perspect Biol 6, a016261 (2014). [PubMed: 25213094]
22. Ghisletti S et al. Identification and characterization of enhancers controlling the inflammatory gene expression program in macrophages. Immunity 32, 317–328 (2010). [PubMed: 20206554]
23. Smale ST, Tarakhovsky A & Natoli G Chromatin contributions to the regulation of innate immunity. Annu Rev Immunol 32, 489–511 (2014). [PubMed: 24555473]
24. Chandel NS Navigating Metabolism. Cold Spring Harbor Laboratory Press, 2015.
25. Broz P & Dixit VM Inflammasomes: mechanism of assembly, regulation and signalling. Nat Rev Immunol 16, 407–420 (2016). [PubMed: 27291964]
26. Wong BW et al. The role of fatty acid β-oxidation in lymphangiogenesis. Nature 542, 49–54 (2017). [PubMed: 28024299]
27. Lee JV et al. Akt-dependent metabolic reprogramming regulates tumor cell histone acetylation. Cell Metab 20, 306–319 (2014). [PubMed: 24998913]
28. Chouchani ET et al. A Unifying Mechanism for Mitochondrial Superoxide Production during Ischemia-Reperfusion Injury. Cell Metab 23, 254–263 (2016). [PubMed: 26777689]
29. Votyakova TV & Reynolds IJ DeltaPsi(m)-Dependent and -independent production of reactive oxygen species by rat brain mitochondria. J Neurochem 79, 266–277 (2001). [PubMed: 11677254]
30. Barrientos A & Moraes CT Titrating the effects of mitochondrial complex I impairment in the cell physiology. J Biol Chem 274, 16188–16197 (1999). [PubMed: 10347173]
31. Chouchani ET et al. Ischaemic accumulation of succinate controls reperfusion injury through mitochondrial ROS. Nature 515, 431–435 (2014). [PubMed: 25383517]
32. Koza RA et al. Sequence and tissue-dependent RNA expression of mouse FAD-linked glycerol-3-phosphate dehydrogenase. Arch Biochem Biophys 336, 97–104 (1996). [PubMed: 8951039]

33. Mráček T, Drahota Z & Houštěk J The function and the role of the mitochondrial glycerol-3-phosphate dehydrogenase in mammalian tissues. Biochim Biophys Acta 1827, 401–410 (2013). [PubMed: 23220394]

34. Garaude J et al. Mitochondrial respiratory-chain adaptations in macrophages contribute to antibacterial host defense. Nat Immunol 17, 1037–1045 (2016). [PubMed: 27348412]

35. Sanin DE et al. Mitochondrial Membrane Potential Regulates Nuclear Gene Expression in Macrophages Exposed to Prostaglandin E2. Immunity 49, 1021–1033.e1026 (2018). [PubMed: 30566880]

36. Weinberg SE, Sena LA & Chandel NS Mitochondria in the regulation of innate and adaptive immunity. Immunity 42, 406–417 (2015). [PubMed: 25786173]

37. Sivanand S, Viney I & Wellen KE Spatiotemporal Control of Acetyl-CoA Metabolism in Chromatin Regulation. Trends Biochem Sci 43, 61–74 (2018). [PubMed: 29174173]

Methods-only references

38. Byles V et al. The TSC-mTOR pathway regulates macrophage polarization. Nat Commun 4, 2834 (2013). [PubMed: 24280772]

39. Salabei JK, Gibb AA & Hill BG Comprehensive measurement of respiratory activity in permeabilized cells using extracellular flux analysis. Nat Protoc 9, 421–438 (2014). [PubMed: 24457333]

40. Liu X, Ser Z & Locasale JW Development and quantitative evaluation of a high-resolution metabolomics technology. Anal Chem 86, 2175–2184 (2014). [PubMed: 24410464]

41. Snyder NW et al. Production of stable isotope-labeled acyl-coenzyme A thioesters by yeast stable isotope labeling by essential nutrients in cell culture. Anal Biochem 474, 59–65 (2015). [PubMed: 25572876]

42. Frey AJ et al. LC-quadrupole/Orbitrap high-resolution mass spectrometry enables stable isotope-resolved simultaneous quantification and (13)C-isotopic labeling of acyl-coenzyme A thioesters. Anal Bioanal Chem 408, 3651–3658 (2016). [PubMed: 26968563]

43. Trefely S, Ashwell P & Snyder NW FluxFix: automatic isotopologue normalization for metabolic tracer analysis. BMC Bioinformatics 17, 485 (2016). [PubMed: 27887574]

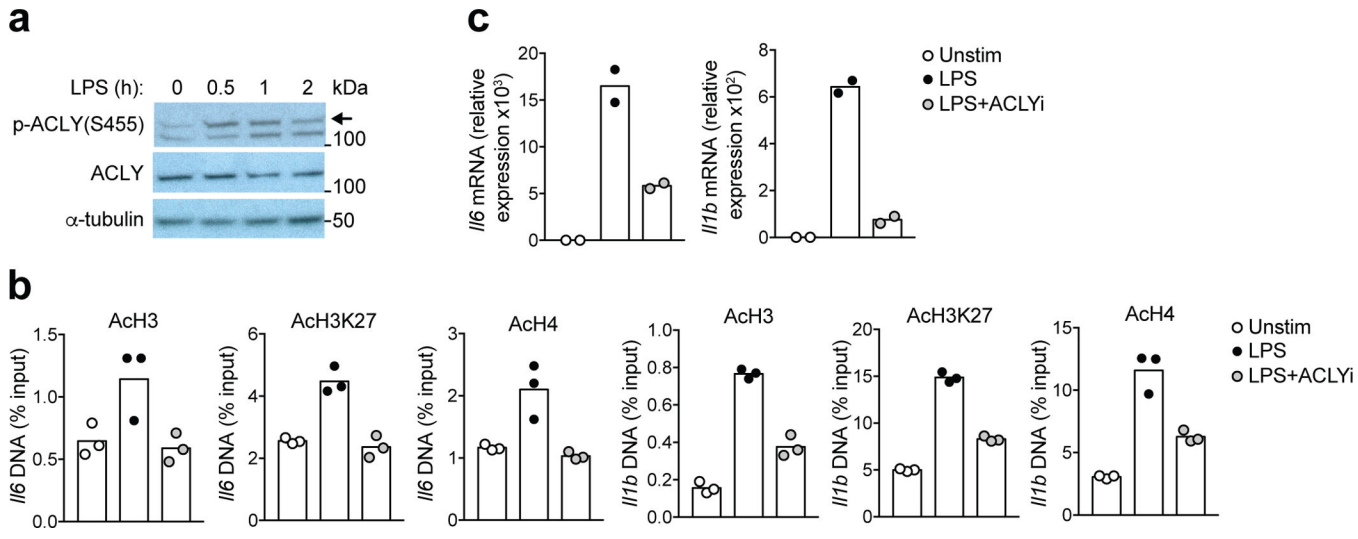

Figure 1.

ACLY activity supports inflammatory gene induction in LPS-activated macrophages. (**a**) Immunoblot analysis of ACLY phosphorylation at Ser455 in BMDMs stimulated with LPS for the indicated times. (**b**) ChIP-qPCR analysis of histone acetylation in *Il6* and *Il1b* promoter regions in BMDMs stimulated with LPS for 0–1h +/− the ACLY inhibitor SB-204990 (ACLYi), 80 μM (n=3). (**c**) qPCR analysis of *Il6* and *Il1b* gene expression in BMDMs stimulated with LPS for 0–3h +/− 80- μM ACLYi (n=2). Data are from one experiment representative of three independent experiments (**a-c**). Mean (**b-c**) shown.

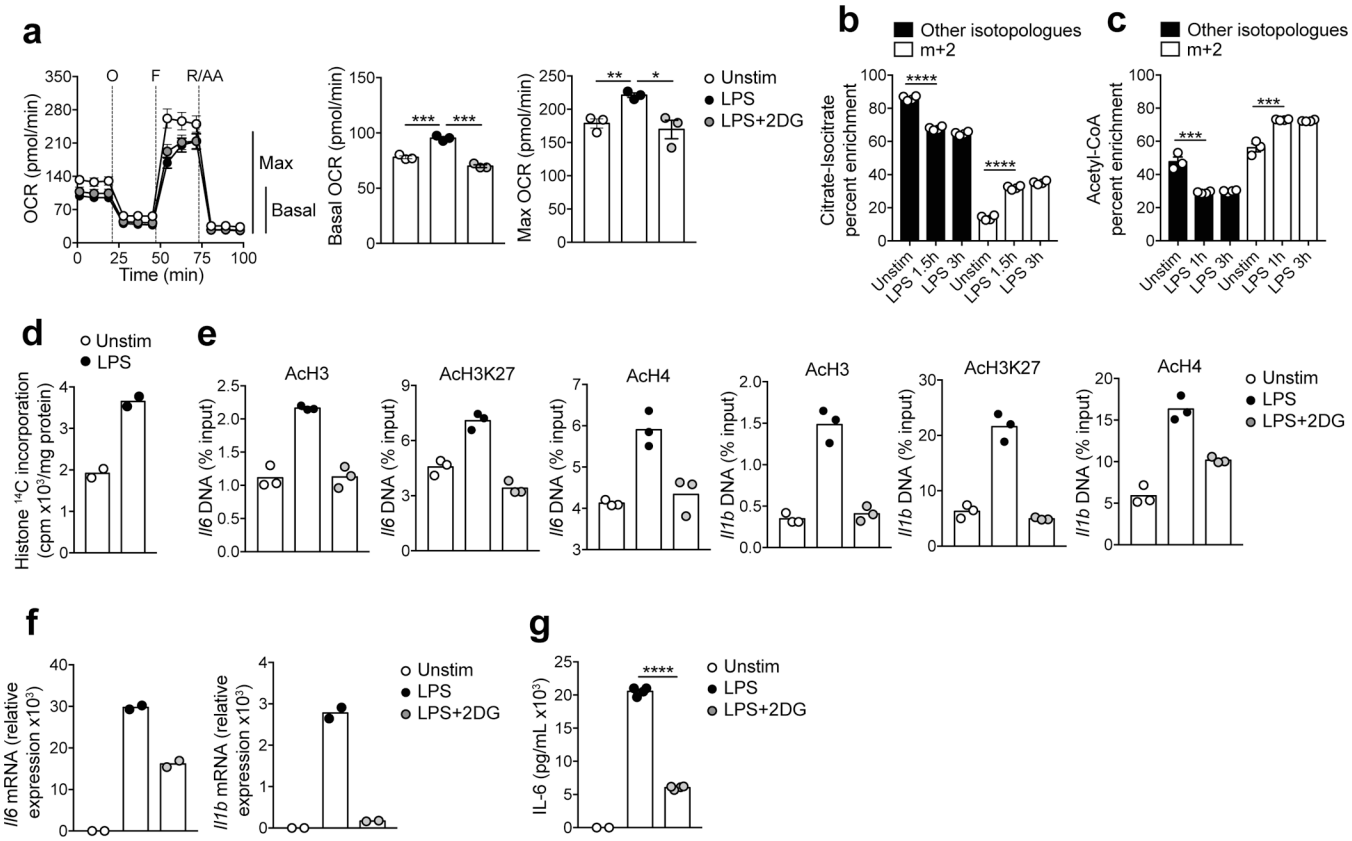

Figure 2.

Glucose oxidation supports inflammatory gene induction in LPS-activated macrophages by providing carbon substrate for histone acetylation. (**a**) Seahorse extracellular flux analysis of oxygen consumption rate (OCR) in BMDMs unstimulated or stimulated with LPS for 1h +/− 2-deoxyglucose (2DG), 10 mM (n=8). Injections were 1 μM oligomycin (O), 1.5 μM FCCP (F), and 2 μM rotenone and 2 μM antimycin A (R/AA). Basal and maximal mitochondrial OCR are shown at right. (**b**,**c**) $^{13}C_6$-glucose tracing into citrate-isocitrate and acetyl-CoA, presented as abundance of m+2 isotopologue relative to all other isotopologues, in BMDMs stimulated with LPS for the indicated times (n=4). (**d**) Tracing of $^{14}C_6$-glucose-derived carbons into histones in BMDMs stimulated with LPS for 0–2h (n=2). (**e**) ChIP-qPCR analysis of histone acetylation in *Il6* and *Il1b* promoter regions in BMDMs stimulated with LPS for 0–1h +/− 10 mM 2DG (n=3). (**f**) qPCR analysis of *Il6* and *Il1b* gene expression in BMDMs stimulated with LPS for 0–3h +/− 10 mM 2DG. (**g**) ELISA for IL-6 production in culture supernatants of BMDMs stimulated and treated as in **f** (n=4). Data are from one experiment representative of ten (**a**), three (**b-d**), or four (**e-g**) independent experiments. Mean (**a-g**) +/− s.e.m. (**a-c**,**g**) shown. *$p \leq 0.05$, **$p \leq 0.01$, ***$p \leq 0.001$, ****$p \leq 0.0001$ (two-tailed Student's *t*-test).

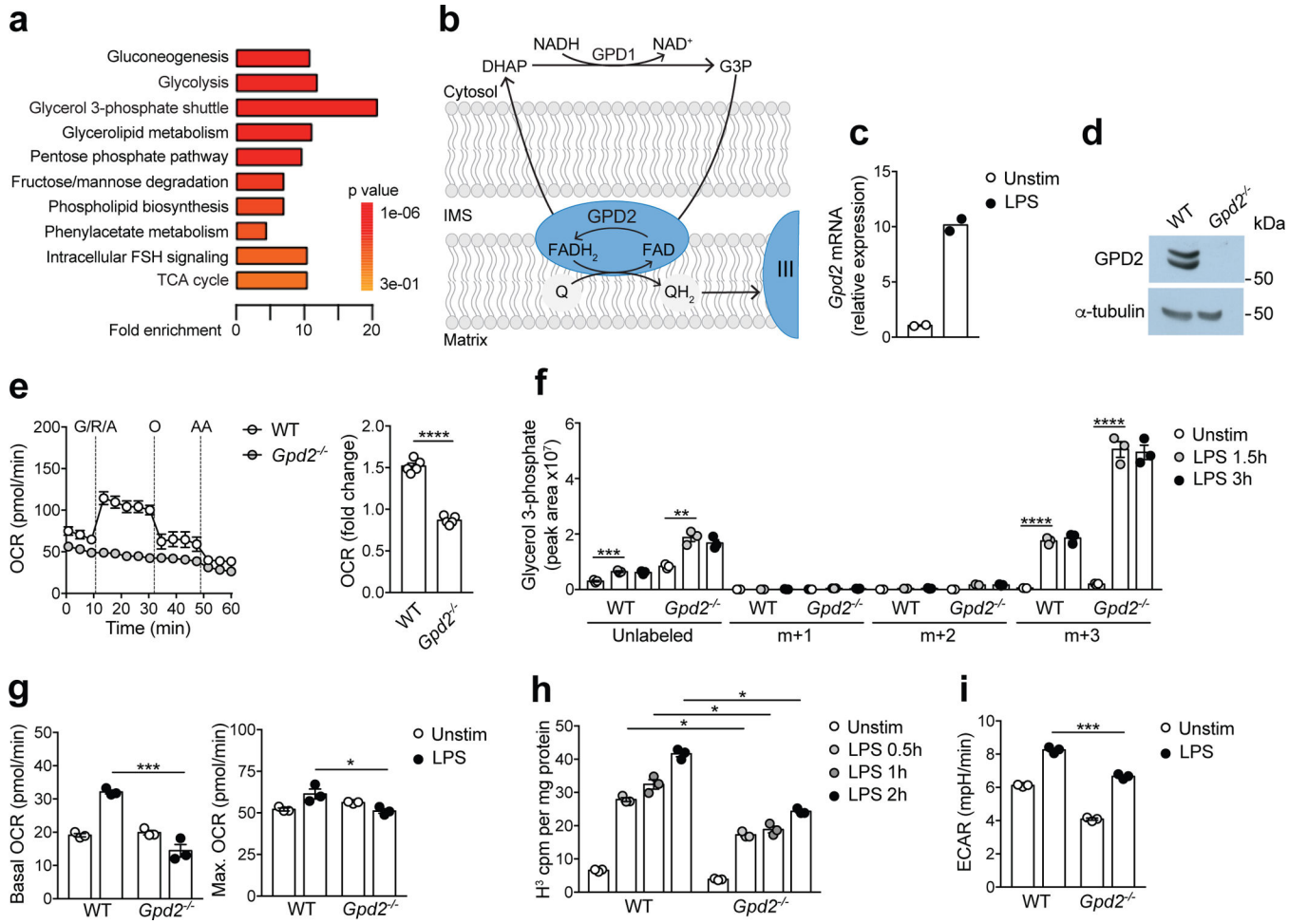

Figure 3.

The GPS enzyme GPD2 regulates glucose oxidation in LPS-activated macrophages. (**a**) Global steady-state metabolite profiling of BMDMs unstimulated or LPS-stimulated for 3h (n=4). Enriched pathways are shown, ranked by *p* value. (**b**) Schematic depicting the spatial and biochemical position of the GPS and GPD2 at the nexus between glycolysis and electron transport. (**c**) qPCR analysis of *Gpd2* gene expression in BMDMs stimulated with LPS for 1.5h. (**d**) Immunoblot analysis of GPD2 in unstimulated wild-type (WT) and *Gpd2*$^{-/-}$ BMDMs. (**e**) Seahorse extracellular flux analysis of OCR in permeabilized WT and *Gpd2*$^{-/-}$ BMDMs (n=6). Injections were 10 mM glycerol 3-phosphate, 2 μM rotenone, 1 mM ADP (G/R/A); 1 μM oligomcyin (O); and 2 μM antimycin A (AA). Bar graph shows fold change in OCR after G/R/A injection. (**f**) $^{13}C_6$-glucose tracing into glycerol 3-phosphate (presented as peak areas for each isotopologue) in WT and *Gpd2*$^{-/-}$ BMDMs (n=3). (**g**) Seahorse analysis of basal and maximal mitochondrial OCR in WT and *Gpd2*$^{-/-}$ BMDMs unstimulated or stimulated with LPS for 1h (n=6). (**h**) Uptake of ^{3}H-deoxy-D-glucose in WT and *Gpd2*$^{-/-}$ BMDMs stimulated with LPS for the indicated times (n=3). (**i**) Seahorse analysis of extracellular acidification rate (ECAR) in WT and *Gpd2*$^{-/-}$ BMDMs stimulated with LPS for 0–2h (n=6). Data are from one experiment representative of two (**a**),

three (**c,d,f-i**), or four (**e**) independent experiments. Mean (**c,e-i**) +/− s.e.m. (**e-i**) shown. *$p \leq 0.05$, **$p \leq 0.01$, ***$p \leq 0.001$, ****$p \leq 0.0001$ (two-tailed Student's *t*-test).

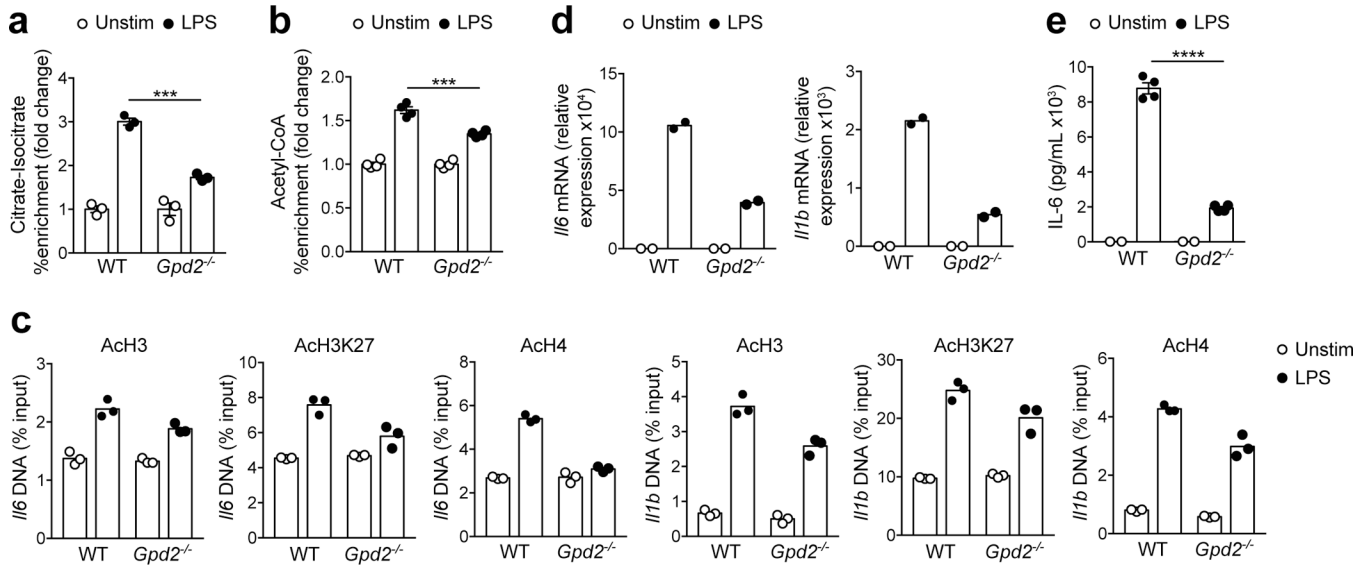

Figure 4.

GPD2 activity influences inflammatory gene induction in LPS-activated macrophages by regulating acetyl-CoA production and histone acetylation. (**a,b**) $^{13}C_6$-glucose tracing into citrate-isocitrate (n=3) and acetyl-CoA (n=4) in WT and *Gpd2*$^{-/-}$ BMDMs, stimulated with LPS for 0–1h, presented as LPS-induced fold change in percent m+2 enrichment. (**c**) ChIP-qPCR analysis of histone acetylation in *Il6* and *Il1b* promoter regions in WT and *Gpd2*$^{-/-}$ BMDMs stimulated with LPS for 0–1h (n=3). (**d**) qPCR analysis of *Il6* and *Il1b* gene expression in WT and *Gpd2*$^{-/-}$ BMDMs stimulated with LPS for 0–3h (n=2). (**e**) ELISA for IL-6 production in culture supernatants of WT and *Gpd2*$^{-/-}$ BMDMs stimulated as in **d** (n=4). Data are from one experiment representative of three (**a,b**) or four (**c-e**) independent experiments. Mean (**a-e**) +/− s.e.m. (**a,b,e**) shown. *$p \leq 0.05$, **$p \leq 0.01$, ***$p \leq 0.001$, ****$p \leq 0.0001$ (two-tailed Student's *t*-test).

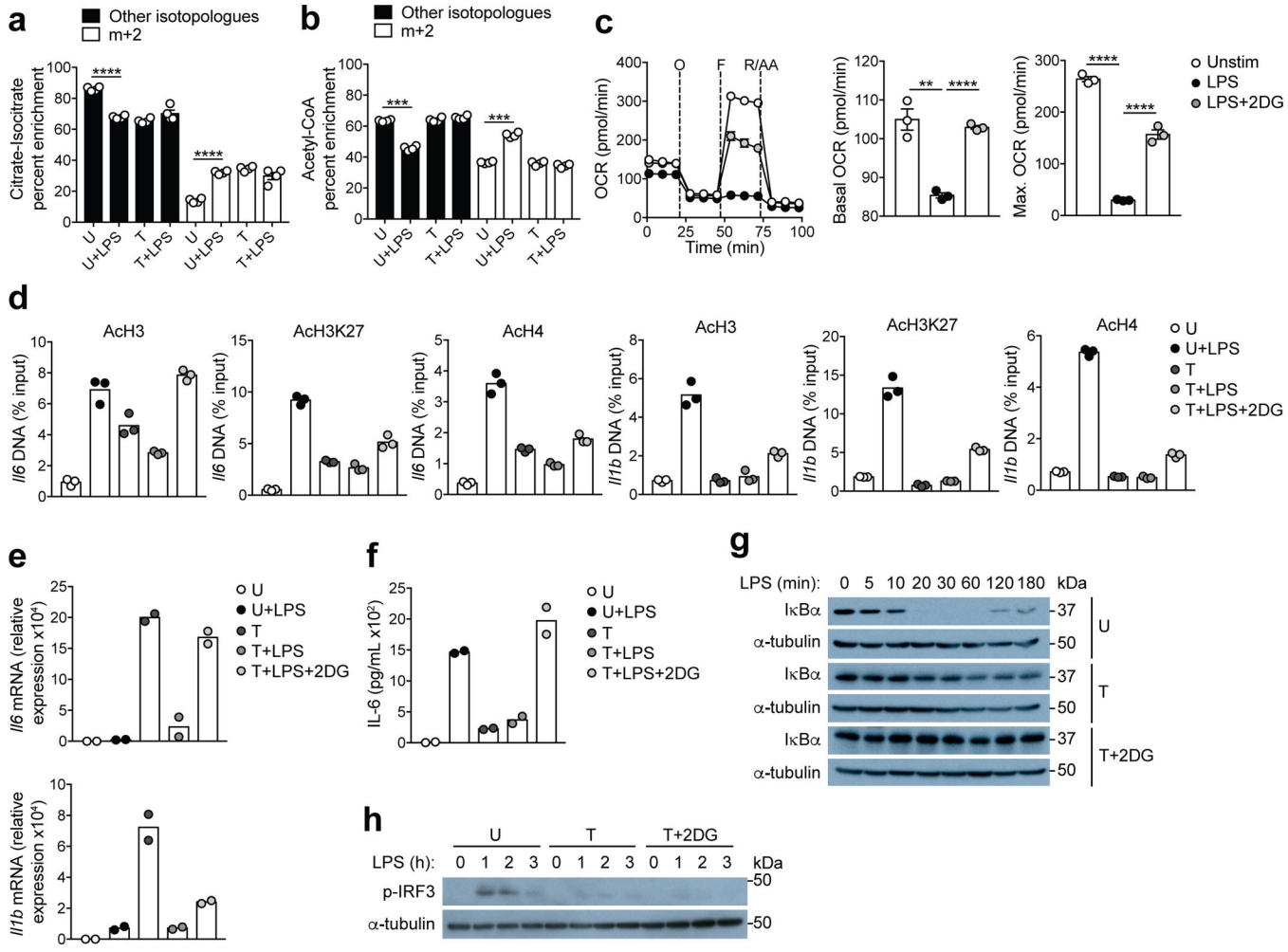

Figure 5.

Glucose utilization impairs oxidative metabolism and limits inflammatory gene induction in tolerant macrophages. (**a,b**) $^{13}C_6$-glucose tracing into citrate-isocitrate and acetyl-CoA, presented as abundance of m+2 isotopologue relative to all other isotopologues, in unstimulated (U) or LPS-stimulated (U+LPS) naïve BMDMs and unstimulated (T) or LPS-stimulated (T+LPS) BMDMs tolerized by 24h LPS stimulation (n=4). (**c**) Seahorse extracellular flux analysis of OCR in BMDMs stimulated with LPS for 12h +/− 5 mM 2DG (n=8). Injections were 1 μM oligomycin (O), 1.5 μM FCCP (F), and 2 μM rotenone and 2 μM antimycin A (R/AA). Basal and maximal mitochondrial OCR are shown at right. (**d**) ChIP-qPCR analysis of histone acetylation in *Il6* and *Il1b* promoter regions in unstimulated (U) or LPS-stimulated (U+LPS) naïve BMDMs and unstimulated (T) or LPS-stimulated BMDMs tolerized by 24h LPS stimulation +/− 5mM 2DG treatment (T+LPS or T+LPS +2DG) (n=3). (**e**) qPCR analysis of *Il6* and *Il1b* gene expression in BMDMs treated as in **d** (n=2). (**f**) ELISA for IL-6 production in culture supernatants of BMDMs treated as in **d** (n=2). (**g,h**) Immunoblot analysis of IκBα degradation and IRF3 phosphorylation at the indicated times following LPS challenge of unstimulated (U) BMDMs or BMDMs tolerized by 24h LPS stimulation +/− 5mM 2DG treatment (T or T+2DG). Data are from one experiment representative of three (**a-d,g,h**) or four (**e,f**) independent experiments. Mean (**a-**

f) +/− s.e.m. (**a-c**) shown. *$p \leq 0.05$, **$p \leq 0.01$, ***$p \leq 0.001$, ****$p \leq 0.0001$ (two-tailed Student's *t*-test).

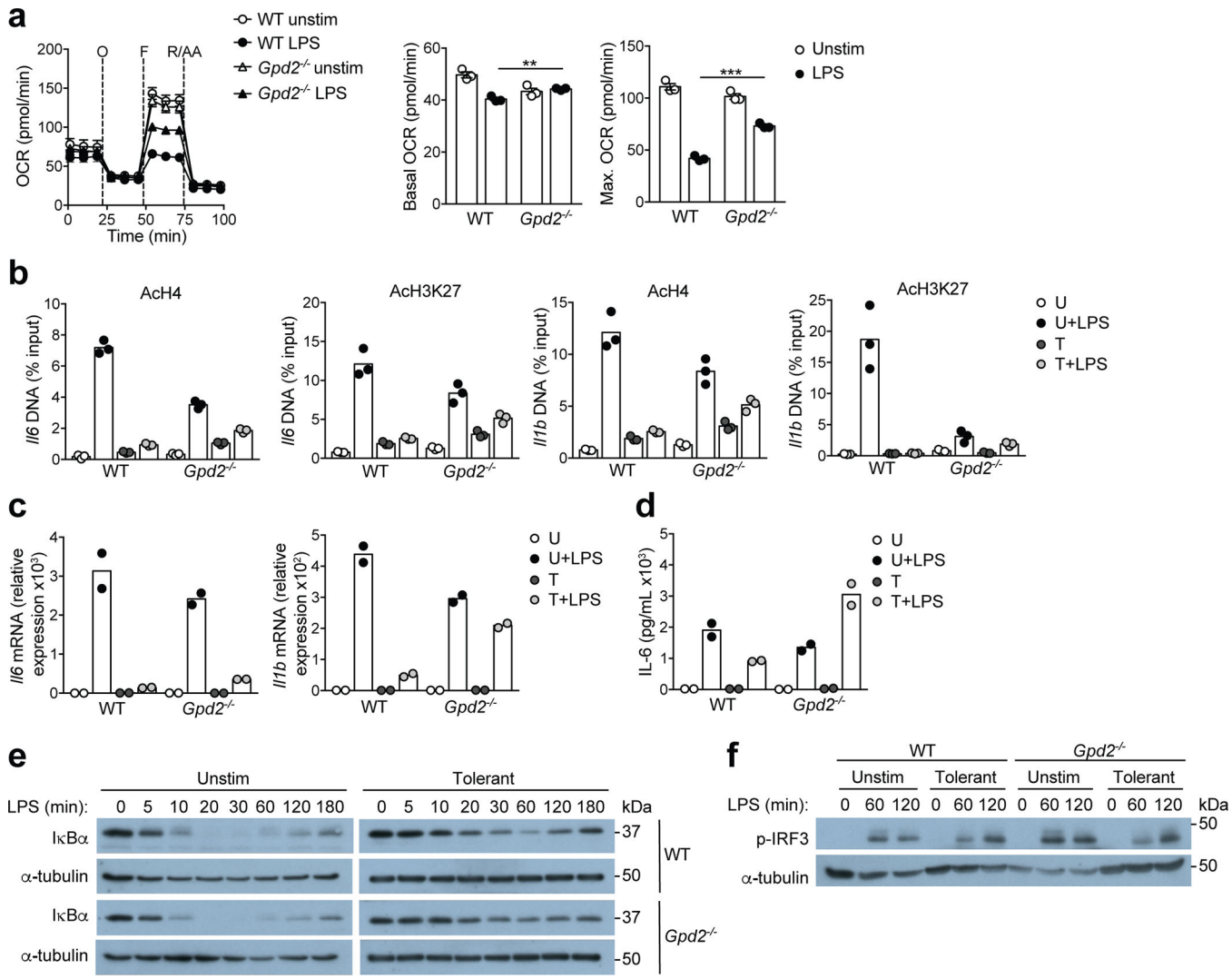

Figure 6.

GPD2 activity influences suppression of inflammatory responses in tolerant macrophages. (**a**) Seahorse extracellular flux analysis of OCR in WT and *Gpd2*$^{-/-}$ BMDMs stimulated with LPS for 12h (n=8). Injections were 1 μM oligomycin (O), 1.5 μM FCCP (F), and 2 μM rotenone and 2 μM antimycin A (R/AA). Basal and maximal mitochondrial OCR are shown at right. (**b**) ChIP-qPCR analysis of histone acetylation in *Il6* and *Il1b* promoter regions in unstimulated (U) or LPS-stimulated (U+LPS) naïve wild-type (WT) and *Gpd2*$^{-/-}$ BMDMs and unstimulated (T) or LPS-stimulated (T+LPS) tolerant WT and *Gpd2*$^{-/-}$ BMDMs (n=3). Tolerance was induced by 24h challenge with LPS, which was washed off before stimulation. (**c**) qPCR analysis of *Il6* and *Il1b* gene expression in BMDMs treated as in **b** (n=2). (**d**) ELISA for IL-6 production in culture supernatants of BMDMs treated as in **b** (n=2). (**e,f**) Immunoblot analysis of IκBα degradation and IRF3 phosphorylation at the indicated times following LPS challenge of WT and *Gpd2*$^{-/-}$ naive (Unstim) BMDMs and BMDMs tolerized by 24h treatment with LPS (Tolerant). Data are from one experiment representative of three independent experiments (**a-f**). Mean (**a-d**) +/− s.e.m. (**a**) shown. *$p \leq 0.05$, **$p \leq 0.01$, ***$p \leq 0.001$, ****$p \leq 0.0001$ (two-tailed Student's *t*-test).

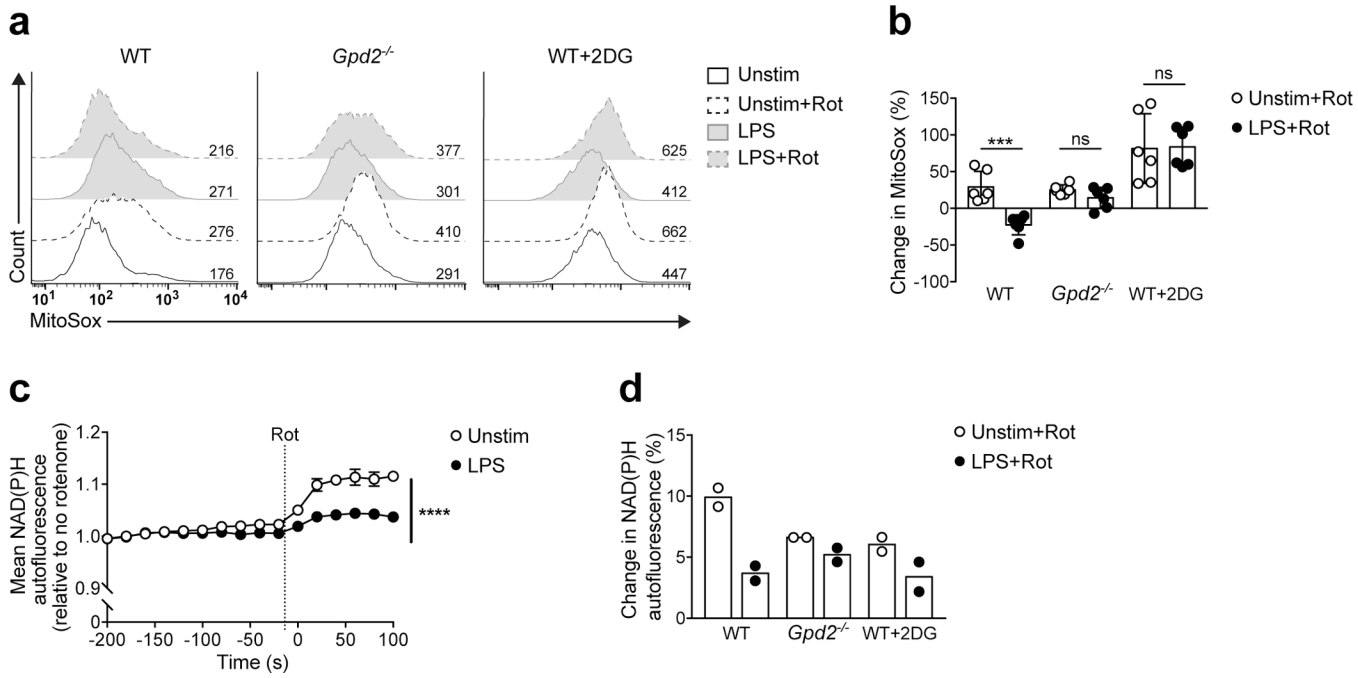

Figure 7.

GPD2-dependent glucose oxidation contributes to reverse electron transport in LPS tolerant BMDMs. (**a,b**) MitoSox labeling of mitochondrial superoxide levels in WT and *Gpd2*$^{-/-}$ BMDMs unstimulated or stimulated with LPS for 12h +/− 5 mM 2DG and +/− 1.5 μM rotenone (Rot), shown as histograms in **a** (numbers are mean fluorescence intensities, MFIs) and as percent change in MitoSox MFI after Rot in **b** (n=6). (**c**) Real-time fluorescence microscopy analysis of NAD(P)H autofluorescence intensity in BMDMs unstimulated or stimulated with LPS for 12h, followed by injection of 1.5 μM Rot (n=100 individual cells). (**d**) NAD(P)H autofluorescence sensitivity to Rot treatment, as measured in **c**, in WT and *Gpd2*$^{-/-}$ BMDMs unstimulated or stimulated with LPS for 12h +/− 5 mM 2DG. Data are from three (**b**) or two (**d**) independent experiments or from one experiment representative of three independent experiments (**a,c**). Mean (**b-d**) +/− s.e.m. (**b,c**) shown. *$p \leq 0.05$, **$p \leq 0.01$, ***$p \leq 0.001$, ****$p \leq 0.0001$ (two-tailed Student's *t*-test).

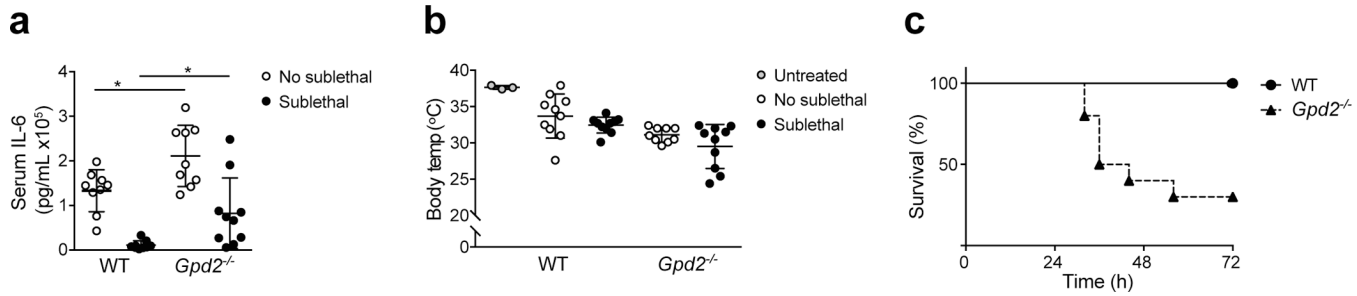

Figure 8.

GPD2 activity supports LPS tolerance *in vivo*. (**a**) ELISA analysis of IL-6 amounts in sera of WT and *Gpd2*$^{-/-}$ mice 6h after a lethal dose of LPS (30 mg/kg), preceded by injection with vehicle (saline) or sublethal LPS (3 mg/kg) 24h before (mean +/− s.d. shown). p=0.0155 (n=9) and p=0.0237 (n=10) respectively for mice without or with sublethal LPS pretreatment; 2way ANOVA with Sidak's multiple comparisons test (*$p \leq 0.05$). (**b**) Mouse internal body temperature 6h after lethal LPS challenge (mean +/− s.d. shown). (**c**) Mouse survival after lethal LPS challenge 24h after sublethal LPS injection. p =0.0012; WT n=20, *Gpd2*$^{-/-}$ n=19; Mantel-Cox test. Data are from two independent experiments (**a-c**).